# Design Formulation for Critical Buckling Stress of Steel Columns Subjected to Nonuniform Fire Loads

MEHRDAD MEMARI and HUSSAM MAHMOUD

## ABSTRACT

Assessing the stability of steel building frames exposed to fire conditions is challenging due to the need to consider elevated temperature properties of steel, nonuniform heating of structural members, and large deformational demands on the frames. There has been significant progress recently in simulating the response of structural members and systems under fire loads using finite element methods. As a result, simple design equations have been developed for predicting the buckling strength of columns under uniform elevated temperature. The equations have been shown to provide accurate predictions and have been adopted by design provisions. There is a need, however, for conducting additional analysis while expanding upon previous work to allow for the development of additional design provisions for column buckling while accommodating varying temperature profiles. This study introduces a framework for conducting stability analyses of W-shape steel columns subjected to demands imposed by fire loads considering nonuniform longitudinal temperature profiles. Results from the analyses show good agreement with available strength design equations of steel columns at ambient and elevated temperatures. An equation is proposed to compute the Euler elastic buckling stress in case of nonuniform longitudinal distribution of temperature. In addition, another equation is proposed to calculate the critical buckling stress of steel columns subjected to nonuniform longitudinal temperature demands. The efficiency of the proposed equations is investigated when two additional nonuniform longitudinal temperature profiles are considered.

**Keywords:** W-shape steel columns, stability analysis, critical buckling stress, fire, nonuniform longitudinal temperature profile.

## RESEARCH BACKGROUND

Significant progress has recently been made in the development of analytical, numerical and experimental tools that can be used to evaluate the response of steel structural members and frames to fire loading. Because columns are key components in resisting gravity loads in a building system, their stability has been the focus of several previous studies (Franssen et al., 1998; Takagi and Deierlein, 2007; Agarwal and Varma, 2011; Morovat et al., 2014). A review of the literature indicates that many experimental studies have been conducted to investigate stability of isolated steel columns under elevated temperatures (e.g., Vandamme and Janss, 1981; Franssen et al., 1998; Ali and O'Connor, 2001). Extensive numerical studies also have been performed to assess the instability of isolated steel columns exposed to fire loads (e.g., Takagi and Deierlein, 2007; Tan and Yuan, 2009; Quiel and Garlock, 2010; Agarwal and Varma, 2011; Agarwal et al., 2014).

Mehrdad Memari, Postdoctoral Fellow, Department of Civil and Environmental Engineering, Colorado State University, Fort Collins, CO. E-mail: Mehrdad.Memari@colostate.edu

Hussam Mahmoud, Associate Professor, Department of Civil and Environmental Engineering, Colorado State University, Fort Collins, CO. E-mail: Hussam.Mahmoud@colostate.edu (corresponding)

Paper No. 2016-18R

Previous experimental fire tests shows that steel columns are typically exposed to nonuniform longitudinal temperature distribution due to the different gas layers in a compartment (Wittheveen and Twilt, 1981; Wang, 2002; Stern-Gottfried et al., 2010; Moinuddin et al., 2011). In addition to experimental work, numerical evaluations conducted by Zhang et al. (2014) demonstrated through simulation of actual fire plumes that the gas temperature for a localized fire are highly nonuniform and that the temperature gradients in steel columns along their length are very evident. Memari and Mahmoud (2014) and Memari et al. (2014) conducted nonlinear finite element analyses to evaluate the performance of steel moment-resisting frames under fire and fire following earthquakes, respectively. These studies highlighted the importance of improving understanding of the buckling response of steel columns subjected to nonuniform longitudinal temperature. All these studies confirmed the presence of thermal gradient along column length and showed that thermal gradient can have a significant negative effect on the response of steel columns exposed to localized fire. The following brief discussion of two of the most recent and relevant studies on steel column buckling under fire (Takagi and Deierlein, 2007; Agarwal and Varma, 2011) will set the stage for introducing the present study for computing the onset of instability of W-shape steel columns under the effects fire loads.

Takagi and Deierlein (2007) evaluated the AISC *Specification* (AISC, 2005) and Eurocode 3 (CEN, 2005) provisions for the design of isolated W-shape steel columns under elevated temperatures that were uniform along the column

length. Numerical models of columns were developed using shell elements, which accounted for residual stresses, local buckling, and material inelasticity. Temperature-dependent material properties were adopted from Eurocode 3 (CEN, 2005). Initial imperfections in the form of out-of-straightness were also considered in the numerical models. It was concluded that the recommendation of the AISC *Specification* (AISC, 2005) to use the ambient temperature design equations in Chapter E for design of axial members under elevated temperatures, modifying only the material properties for elevated temperatures, was highly nonconservative. The outcome of this study was the design equation for W-shape steel columns under uniform longitudinal temperature that currently appears in Appendix 4, Equation A-4-2, of the AISC *Specification* (AISC, 2010; AISC, 2016).

Following the significant work by Takagi and Deierlein (2007), Agarwal and Varma (2011) subsequently conducted comprehensive finite element analyses to evaluate the effects of slenderness and rotational restraints on the buckling response of W-shaped steel columns subjected to uniform elevated temperatures. Shell elements were used to create numerical models of columns because of their ability to capture local buckling and inelastic flexural-torsional buckling and to accommodate the specified residual stress distribution. Initial geometric imperfections, representing out-of-straightness, were included in the models as well as local imperfections. As with the earlier Takagi and Deierlein (2007) study, temperature-dependent stress-strain curves from Eurocode 3 (CEN, 2005) were implemented in the numerical models. This study resulted in new design equations for steel columns with uniform longitudinal temperature distribution considering an equivalent bilinear material behavior. The effects of rotational restraints, provided by continuity with cooler columns above and below the column of interest in a structural frame, were also included in the proposed design equations.

The studies by Takagi and Deierlein (2007) and Agarwal and Varma (2011) provided a solid foundation for evaluating steel columns under fire. These studies showed that the computational efforts associated with analyzing the stability of columns at elevated temperatures were quite substantial. To minimize these efforts, the two aforementioned studies introduced a number of assumptions and simplifications to reduce the number of analyses so that the computational effort for developing the design equations is minimized. For instance, the effects of nonuniform longitudinal temperature, various boundary conditions, and out-of-plumbness imperfection effects were excluded from the studies. Therefore, there remains a need for simple design equations that can be utilized to evaluate the instability of columns under nonuniform longitudinal fire loads while accounting for material inelasticity and geometric nonlinearity associated with column behavior under elevated temperature conditions.

In the current study, a set of equations is proposed for predicting the instability of W-shape steel columns subjected to nonuniform longitudinal temperature profiles caused by fire. To do so, a nonlinear finite element approach is employed that takes into account the temperature-dependent residual stress distribution in steel hot-rolled W-shape sections, initial out-of-straightness and out-of-plumbness in steel members, temperature-dependent material properties, and specified boundary conditions. The results of the finite element analysis (FEA) are first verified against comparison with previous studies. Afterward, equations are proposed for predicting the Euler elastic buckling stress as well as the critical buckling stress as a function of the Euler elastic stress in steel columns subjected to fire loads, represented by nonuniform longitudinal temperature distributions.

## ANALYSIS FRAMEWORK

A finite element approach is implemented to predict the onset of instability of steel columns subjected to variable temperature distribution along their length. The Euler-Bernoulli beam theory is employed to consider constant temperature throughout the cross-section of the column. This approach is an extension of studies conducted by Carol and Murcia (1989), Memari and Attarnejad (2010), and Memari et al. (2017). In this method, a finite element is assumed to have a nonuniform longitudinal temperature distribution with $T_i$ and $T_j$ being the nodal temperatures at either end as shown in Figure 1. Because the elastic modulus of structural steel is a function of temperature and degrades at elevated temperatures, the nodal temperature at each end of the finite element will result in temperature-dependent modulus of elasticity $E(T_i)$ and $E(T_j)$ in accordance with Figure 1(a). A linear variation of temperature-dependent modulus of elasticity is assumed along the length of the finite element per Equation 1, in which $\zeta$ is determined according to Equation 2. The entire column can be then divided into a sufficient number of elements such that the linear variation along each finite element allows the nonlinear variation along the entire length of the column to be captured.

$$E(x) = E(T_i)\left(1 + \frac{\zeta x}{L}\right) \tag{1}$$

where

$$\zeta = \frac{E(T_j)}{E(T_i)} - 1 \tag{2}$$

In this approach, three sets of equations are considered, including kinematic, second-order equilibrium, and constitutive law equations. In accordance with the deformed state of the finite element, shown in Figure 1(b), the kinematic equations, relating the displacements to the strain and

rotation fields are developed in a matrix and compact form per Equations 3 and 4, respectively, as follows:

$$\begin{bmatrix} -(u_j - u_i) \\ \dfrac{w_j - w_i}{L} - \theta_i \\ \theta_j - \dfrac{w_j - w_i}{L} \end{bmatrix} = \int_0^L \begin{bmatrix} 1 & 0 \\ 0 & 1 - \dfrac{x}{L} \\ 0 & \dfrac{x}{L} \end{bmatrix} \begin{bmatrix} \varepsilon \\ \phi \end{bmatrix} dx \quad (3)$$

$$u = \int_0^L \Omega^T \gamma \, dx \quad (4)$$

where ε and ϕ are the axial strain at the neutral axis of the cross-section and curvature, respectively, and other variables in Equation 3 are shown in Figure 1(b). In Equation 4, $u$ demonstrates a vector of relative displacements and rotations, Ω is a transformation matrix that converts strains to displacements and rotations, and γ is the vector of strains.

The cross-sectional axial force, $N(x)$, and bending moment, $M(x)$, can be determined based on applied nodal axial force, $N_i$, and nodal moments, $M_i$ and $M_j$, using equilibrium equations per Equation 5 and its compact form according to Equation 6. To include the second-order ($P$-δ) effects, a vector of forces due to the deformed state of the finite element, shown in Figure 1(c), is added to the nodal equilibrium equations as shown:

$$\begin{bmatrix} N(x) \\ M(x) \end{bmatrix} = \begin{bmatrix} 1 & 0 & 0 \\ 0 & 1 - \dfrac{x}{L} & \dfrac{x}{L} \end{bmatrix} \begin{bmatrix} N_i \\ M_i \\ M_j \end{bmatrix} + \begin{bmatrix} 0 \\ -N_i w_2(x) \end{bmatrix} \quad (5)$$

$$R(x) = \Omega f + R_2(x) \quad (6)$$

where $w_2(x)$ is the out-of-straightness curvature of the beam-column finite element that causes the $P$-δ effects. In Equation 6, $R(x)$ is a vector of internal cross-sectional forces developed at the inclusion of second-order effects, $R_2(x)$. The vector $f$ represents the applied nodal forces and moments and Ω is a matrix that correlates the applied nodal forces to those developed internally in the cross-section. It can be seen that the matrix Ω appears in both the kinematic and equilibrium equations. In addition, the cross-sectional strain and curvature must be related to the cross-sectional forces and moments per Equation 7 (compact form, Equation 8) under the assumption that the element responds elastically to nodal forces:

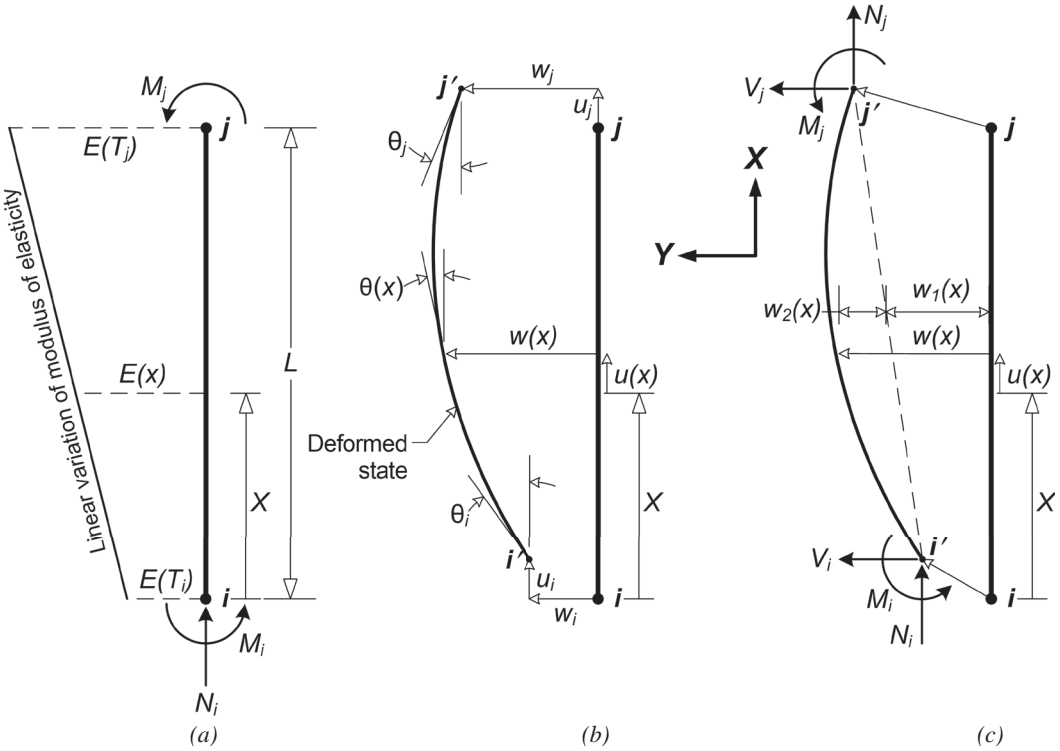


*Fig. 1. (a) A finite element subjected to nonuniform longitudinal temperature and three applied external nodal forces; (b) the deformed state of the finite element with all nodal deformation variables; (c) the deformed state of the finite element with all nodal force variables.*

$$\begin{bmatrix} N(x) \\ M(x) \end{bmatrix} = \begin{bmatrix} E(x)A & 0 \\ 0 & E(x)I \end{bmatrix} \begin{bmatrix} \varepsilon \\ \phi \end{bmatrix} \tag{7}$$

$$R(x) = k_s(x)\gamma \tag{8}$$

where $A$ and $I$ are the cross-sectional area and moment of inertia, respectively, and $k_s(x)$ is the cross-sectional stiffness matrix. The remaining variables were defined previously. It is noted that the longitudinal variation in the modulus of elasticity, caused by the nonuniform temperature distribution, is reflected in Equation 9 by substituting the longitudinal linear variation of the elastic modulus, Equation 1. This is one of the most important features of the presented framework because a constant modulus of elasticity would imply no variation in temperature along the length. Equation 9 clearly indicates that the section stiffness varies along the length of element as a function of the elastic modulus:

$$k_s(x) = E(T_i)\left[1 + \frac{\zeta x}{L}\right]\begin{bmatrix} A & 0 \\ 0 & I \end{bmatrix} \tag{9}$$

The first-order stiffness and geometric stiffness matrices necessary for the stability analysis can be extracted from the three sets of kinematic, equilibrium, and material law equations by substituting the equilibrium, Equation 6, and constitutive, Equation 8, equations into the kinematic equation, Equation 4. Further details are provided in Memari (2016) and Memari et al. (2017). In summary, the stiffness and geometric stiffness matrices of a beam-column finite element are developed to reflect nonuniform temperature variation along the length of the discrete elements when considering a uniform temperature distribution through the cross-section. Figure 2 shows a schematic description of the finite element model of a steel column under an arbitrary longitudinal distribution of temperature. It is noted that all columns analyzed in this study are divided into 50 identical elements in length. The assemblage of stiffness matrices (first-order and geometric) of all 50 elements resulted in the stiffness matrix of the whole column.

No initial imperfection is introduced to the column in the linear elastic analysis; however, sources of initial imperfection including out-of-straightness, as shown in Figure 2(a), and out-of-plumbness are independently considered in the geometry of the columns in the nonlinear inelastic analysis. The out-of-straightness is modeled by introducing a single sinusoidal curve along the column length such that a maximum displacement of $0.001L_c$—per Commentary Section C2 in the AISC *Specification* (AISC, 2016)—is located at mid-height of column, where $L_c$ is the length of column. The effect of out-of-plumbness is also included explicitly in the finite element analysis. Specifically, an initial out-of-plumbness of $0.001L_c$—below the allowable limit of $0.002L_c$ per Commentary Section C2 in the AISC *Specification*—is assumed at the top of the column, and the lateral nodal displacement for the remaining nodes is calculated assuming a straight column. Following this step, the lateral nodal displacements are multiplied by the applied axial force to compute the corresponding nodal moments, which are then assembled with the applied axial force to form the entire action vector on the column. Figures 2(b) and 2(c) show how the nonuniform longitudinal temperature profile and angle of finite elements are incorporated in formation of stiffness matrices.

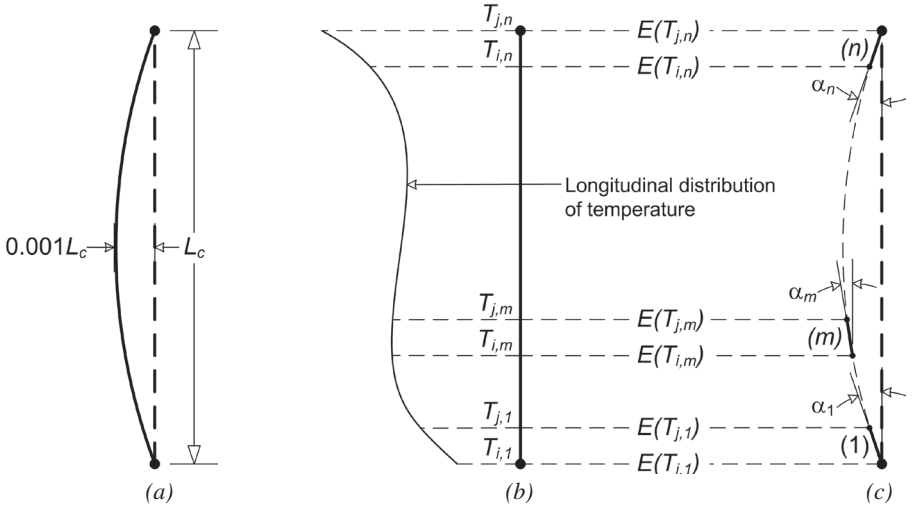


*Fig. 2. (a) The inclusion of out-of-straightness initial imperfection with a single sinusoidal curve along the length of column; (b) nonuniform longitudinal distribution of temperature in the column; (c) schematic explanation of finite element analysis considering angle of elements.*

| Table 1. Longitudinal Variation of Mechanical Properties of Structural Steel According to Nonuniform Temperature Profiles | | | | | |
|---|---|---|---|---|---|
| | | | $\chi_{prop}$, Longitudinal Reduction of Mechanical Properties between Cool and Hot Ends of Steel Column (%) | | |
| Profile | Temperature at Cool End, °F (°C) | Temperature at Hot End, °F (°C) | Modulus of Elasticity, ksi | Yield Stress, ksi | Proportional Limit |
| 1 | 68 (20) | 572 (300) | 20.0 | 0.0 | 38.7 |
| 2 | 392 (200) | 932 (500) | 33.3 | 22.0 | 55.4 |
| 3 | 572 (300) | 1112 (600) | 61.3 | 53.0 | 70.6 |
| 4 | 752 (400) | 1472 (800) | 87.1 | 89.0 | 88.1 |

The stress-strain curve is assumed to have an elastic–perfectly plastic behavior at ambient temperature, 68°F (20°C). At elevated temperatures, the transition from elastic to inelastic material behavior utilized has a significant effect on the calculated critical buckling stress of steel columns (Takagi and Deierlein, 2007; Agarwal and Varma, 2011). Therefore, the modulus of elasticity is only considered in the elastic buckling analysis, while three mechanical properties of structural steel are considered in the inelastic instability analysis of columns exposed to elevated temperatures: modulus of elasticity, $E$, proportional limit, $F_p$, and yield stress, $F_y$. Temperature-dependent mechanical properties of structural steel are modeled as in Eurocode 3 (CEN, 2005), as shown in Figure 3(a). This material modeling approach was also implemented by Takagi and Deierlein (2007). The variations in $E$, $F_p$ and $F_y$ as a function of temperature, described by $\beta_E$, $\beta_p$ and $\beta_y$, respectively, from Eurocode 3 stress-strain curves are shown in Figure 3(b). In addition, it is noted that the temperature-dependent material properties according to Eurocode 3 inherently capture creep effects.

## TEMPERATURE PROFILES

A uniform temperature is assumed across the W-shape steel section in accordance with design recommendations by the AISC *Specification* (AISC, 2016), Takagi and Deierlein (2007), and Agarwal and Varma (2011). The uniform longitudinal temperature profiles will be used for validation analyses. In the current study, four various nonuniform longitudinal temperature profiles are considered in the steel columns as shown in Table 1, which summarizes longitudinal reduction of temperature-dependent mechanical properties from the cool end to the hot end of a steel column. The temperature intervals were selected such that they

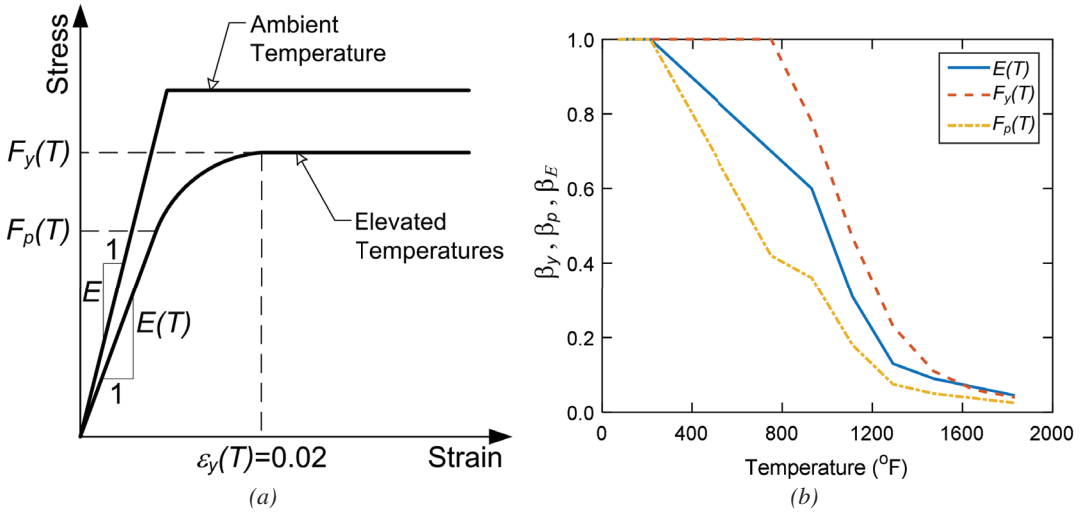


*Fig. 3. Schematic explanation of material modeling: (a) Eurocode 3; (b) variations in modulus sof elasticity, yield stress, and proportional limit in accordance with Eurocode 3 (CEN, 2005).*

capture various rates of longitudinal change in temperature-dependent mechanical properties of structural steel according to Equation 10:

$$\chi_{prop} = \frac{Q(T_{cool-end}) - Q(T_{hot-end})}{Q(T_{cool-end})} \quad (10)$$

where $Q(T_{cool-end})$ and $Q(T_{hot-end})$ represent temperature-dependent mechanical properties at the cool and hot ends of the steel column, respectively, and $\chi_{prop}$ indicates the longitudinal reduction of mechanical properties between the cool and hot ends of the steel column.

These four nonuniform longitudinal temperature distributions are suited for the evaluation of instability of steel columns under different levels of variation in mechanical properties of structural steel as shown in Figure 4. It is emphasized that these nonuniform longitudinal temperature profiles are not the results of any heat transfer analysis.

The pattern of temperature distribution along the length of a column is also an important parameter to be considered. A quick glance into the solution of the governing one-dimentional partial differential equation (PDE) for heat transfer through conduction, Equation 11, shows heat distribution to follow a parabolic function along the length of steel member at time $t$:

$$\frac{\partial T(x,t)}{\partial t} = \alpha(T)\frac{\partial^2 T(x,t)}{\partial x^2} \quad (11)$$

where $T$ is temperature in °F (°C), $x$ is the coordinate axis along the length of column, and $\alpha(T)$ is thermal diffusivity as a function of temperature. Hence, it is essential to evaluate instability of steel columns with parabolic distribution of temperature along their length. However, because the requirements in code provisions to solve conduction heat-transfer PDE problems and obtain a parabolic distribution of temperature along the length of the member pose difficulties in real applications, a linear longitudinal distribution of temperature will be also considered. This is done to evaluate the difference in the results when using the two different patterns of temperature distribution and assess that the effect of using a linear distribution on the results is within what might be considered acceptable. This will also allow for understanding the difference resulting from using a simplified linear distribution on instability analysis of steel columns under fire. These two patterns of nonuniform longitudinal temperature profiles are shown in Figure 5.

Both parabolic and linear longitudinal distributions of temperature in steel columns can be calculated according to Equation 12, in which $\eta$ is determined per Equation 13, as follows:

$$T(x) = T_{cool-end}\left(1 + \frac{\eta x}{L_c}\right)^b \quad (12)$$

$$\eta = \frac{T_{hot-end}}{T_{cool-end}} - 1 \quad (13)$$

where $x$ is the coordinate axis along the length of column from 0 to $L_c$, $T_{cool-end}$ and $T_{hot-end}$ represent temperature at the cooler and hotter ends of the column, and $b$ determines the degree of polynomial such that it is 2 for parabolic and 1 for linear functions. Table 2 summarizes values for $\eta$ in Equation 12 for all four longitudinal temperature profiles shown in Figure 5.

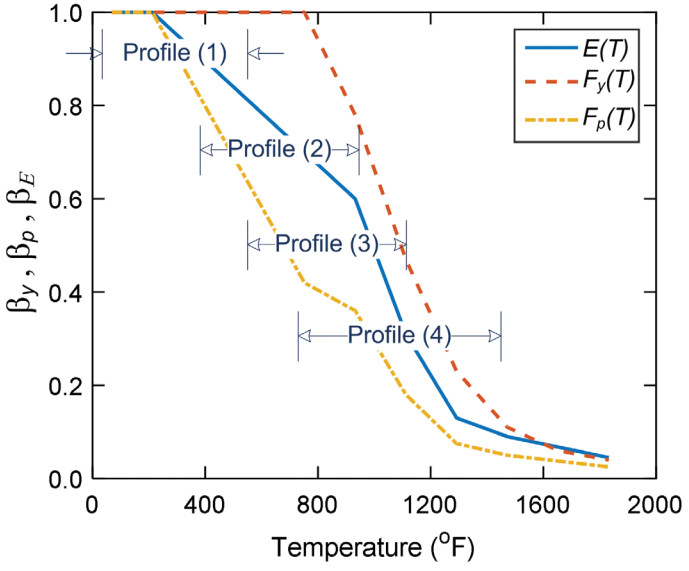


*Fig. 4. Temperature intervals in the nonuniform longitudinal temperature profiles.*

| Table 2. Values of η for Both Parabolic and Linear Temperature Profiles | |
|---|---|
| **Profile** | **η** |
| 1 | 14 |
| 2 | 1.5 |
| 3 | 1.0 |
| 4 | 1.0 |

## LINEAR ELASTIC ANALYSIS

This section presents details of the linear elastic finite element analysis used to obtain the Euler elastic critical stress for a column subjected to nonuniform longitudinal temperature distribution. A modal analysis (eigenvalue analysis) is performed to determine eigenvalues (elastic buckling force) and eigenvectors (elastic buckling mode shapes). Furthermore, the effective length factor of column buckling can be calculated for the first mode shape and higher. To solve the buckling eigenvalue problem, Equation 14 needs to be considered as follows:

$$\left[K_E + \mu K_G\right]\{X\} = \mu\{X\} \tag{14}$$

where μ will return the eigenvalue and $\{X\}$ is the corresponding eigenvector. For the column elastic buckling analysis, $K_E$ represents the first-order stiffness matrix, and $K_G$ is the second-order (geometric) stiffness matrix. A nontrivial solution exists for Equation 14 if and only if

$$\left|K_E + \mu K_G\right| = 0 \tag{15}$$

It is essential to validate both stiffness matrices of a steel column by running an eigenvalue problem with known results. To do so, a uniform longitudinal temperature

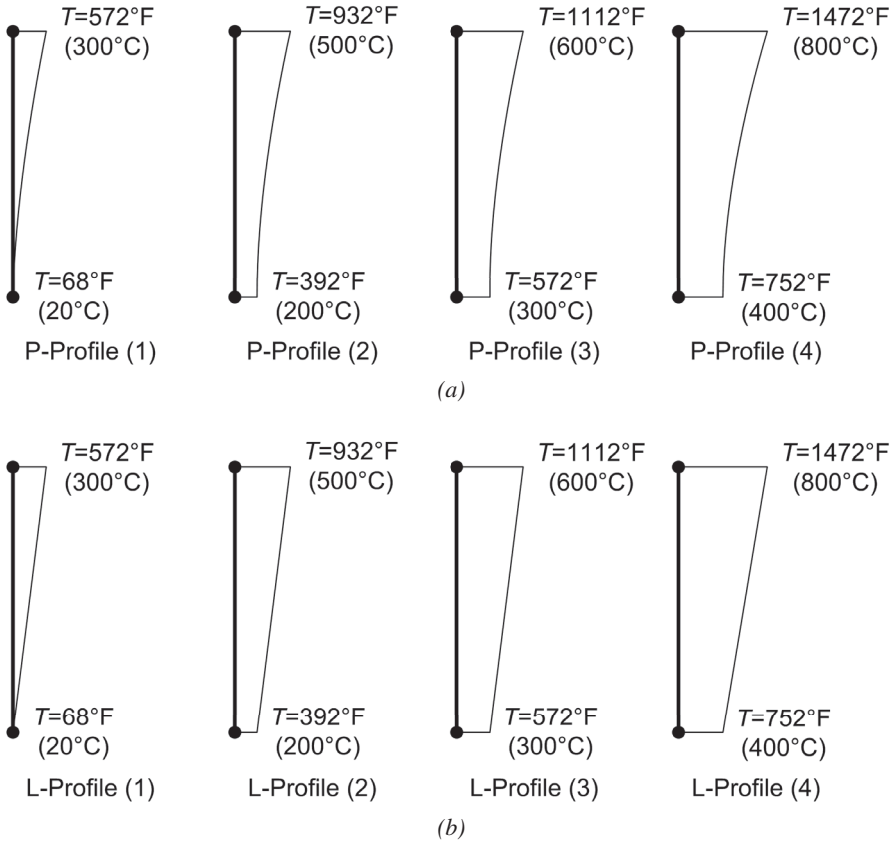


*Fig. 5. (a) Parabolic and (b) linear nonuniform distribution of temperature along the length of column.*

distribution—for example, 572°F (300°C)—is considered to compute the Euler elastic buckling stress for a column with a pinned-pinned boundary condition. This will allow for direct comparison between the results of the eigenvalue problem and the equation of Euler elastic buckling stress, Equations 16 and 17, as follows:

$$F_e(T) = \frac{\pi^2 E(T)}{\lambda^2} \tag{16}$$

$$\lambda = \frac{KL_c}{r} \tag{17}$$

where $F_e(T)$ is the Euler elastic buckling stress as a function of temperature, $E(T)$ is the temperature-dependent modulus of elasticity, $\lambda$ is slenderness of column, $K$ is the effective length factor, $L_c$ is the length of column, and $r$ is the radius of gyration of the column section. Figure 6 shows that Euler elastic buckling stress about both strong and weak axes of a W14×90 steel section using finite element analysis is in excellent agreement with the results of the Euler equation (Eq. 16). This validates both the first-order and geometric stiffness matrices generated based on the proposed finite analysis approach in the current study.

In the linear elastic analysis, the effects of both uniform and nonuniform longitudinal temperature profiles, along with boundary conditions on elastic buckling force and mode shapes of steel columns, are assessed. In the context of this study, only the first eigenvalue (Euler elastic buckling force) and the first three eigenvectors (mode shapes) are discussed here. The first three mode shapes of instability of the steel column with various parabolic longitudinal temperature profiles and boundary conditions are shown in Figure 7. It should be noted that the black dashed lines show instability mode shapes when the uniform longitudinal temperature distribution is used. It is observed that nonuniform longitudinal temperature distributions change the instability mode shape of steel column although this change is insignificant in profiles 1, 2 and 3. Table 1 shows that longitudinal reduction of material stiffness (elastic modulus) is up to 61.3% in profiles 1, 2 and 3. However, profile 4 shows a significant change in mode shapes of instability in comparison to those produced using uniform longitudinal temperature distribution or nonuniform temperature in profiles 1, 2 and 3. This can be attributed to the fact that the modulus of elasticity has a longitudinal variation of 87.1% in profile 4. This difference is larger in higher mode shapes of instability for example, the third mode shape shown in Figure 7. In general, the three mode shapes indicate that maximum deflection along column length is shifted toward higher temperature zones (i.e., softer material) while naturally accounting for the effect of boundary conditions.

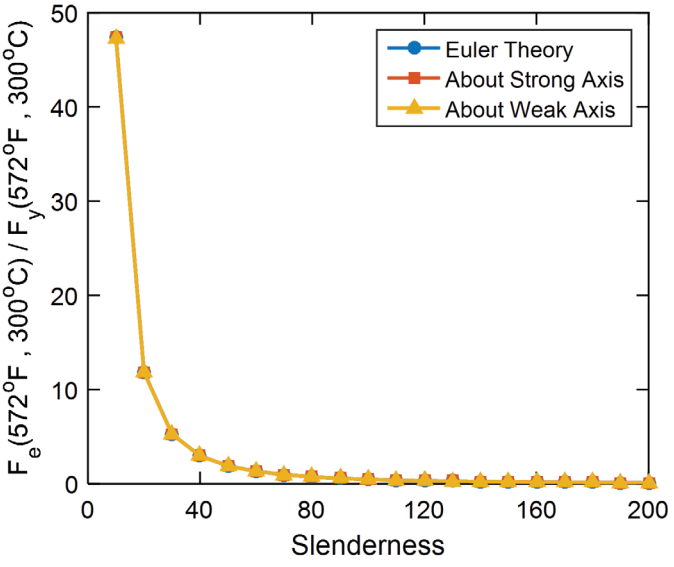


*Fig. 6. Euler elastic buckling stress computed by finite element approach presented in this study and the Euler equation.*

It is also important to assess the effects of parabolic and linear variation of temperature distribution along the length of column on the mode shapes of instability. Figure 8 shows the mode shapes of instability for both parabolic and linear longitudinal variation of temperature using fixed-fixed and pinned-fixed boundary conditions. Figure 8(a) shows the first three mode shapes of instability for linear longitudinal temperature distribution and fixed-fixed boundary conditions, while Figure 8(b) displays them for a parabolic longitudinal temperature profile and fixed-fixed boundary condition. In addition, Figures 8(c) and 8(d), respectively, show the first three mode shapes of instability for linear and parabolic longitudinal variation of temperature considering a pinned-fixed boundary condition (BC). The results of the analysis show that at least under elastic conditions, parabolic and linear longitudinal variations of temperature make no difference on mode shapes of instability. This will be further investigated in the section discussing nonlinear inelastic stability analysis.

The effective length factor, $K$, for the first mode shape is calculated based on curvature (second derivative of deformation) change along the length of column. The results of the calculations are summarized in Table 3. The effective length factors listed in the table for uniform longitudinal temperature profiles correspond to the values available in the literature. As shown in Table 3, the effective length factors change slightly in profiles 1, 2 and 3 as expected because the change in mode shapes was minimal due to these profiles. The change in effective length factors is relatively significant in profile 4, which confirms mode shapes observed previously in Figure 7. It is noted that the calculated effective length factors in accordance with Table 3 are in compliance with

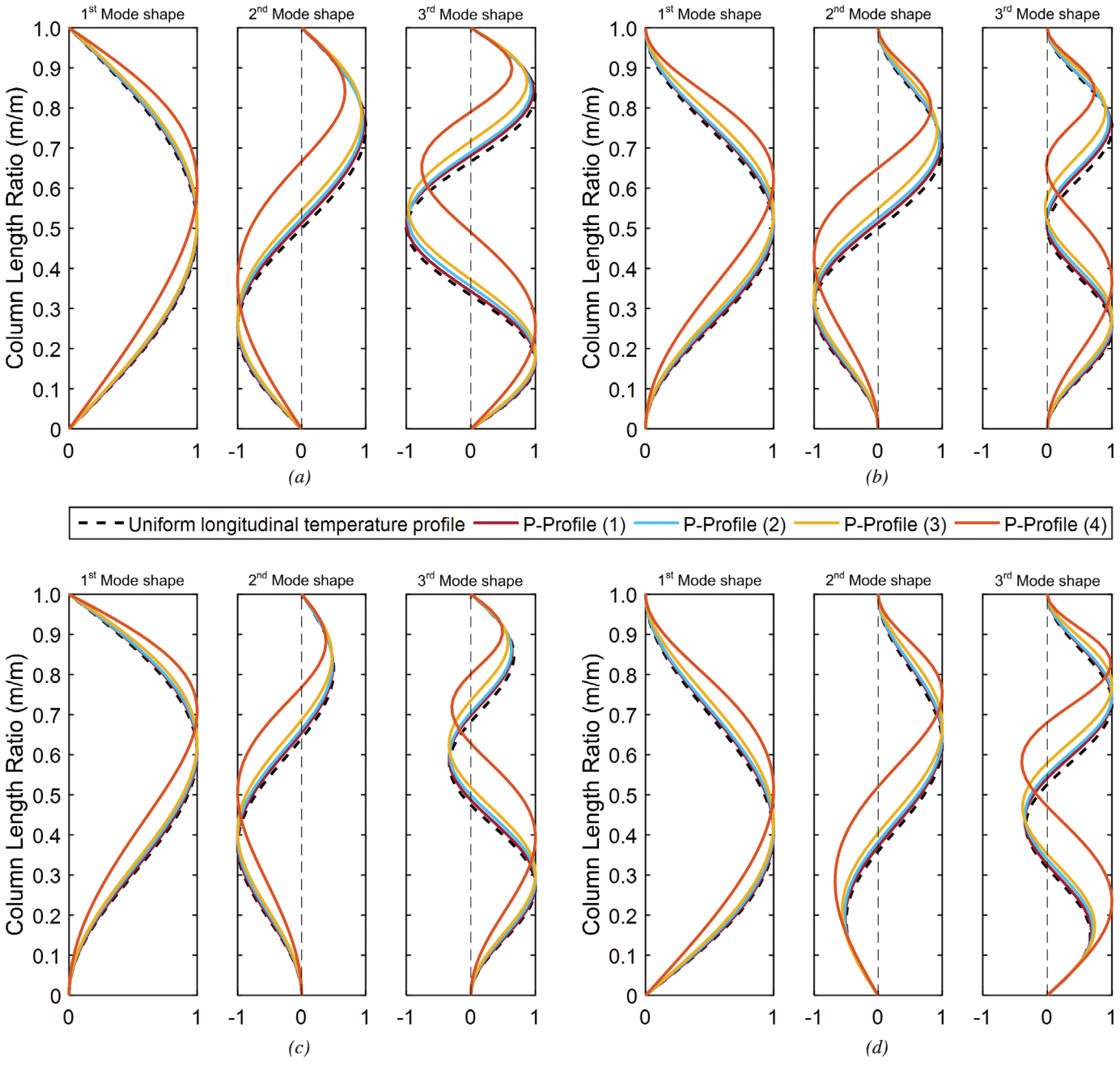


*Fig. 7. The first three mode shapes of instability in the steel column with various parabolic longitudinal temperature distributions: (a) pinned-pinned; (b) fixed-fixed; (c) fixed-pinned; (d) pinned-fixed boundary conditions.*

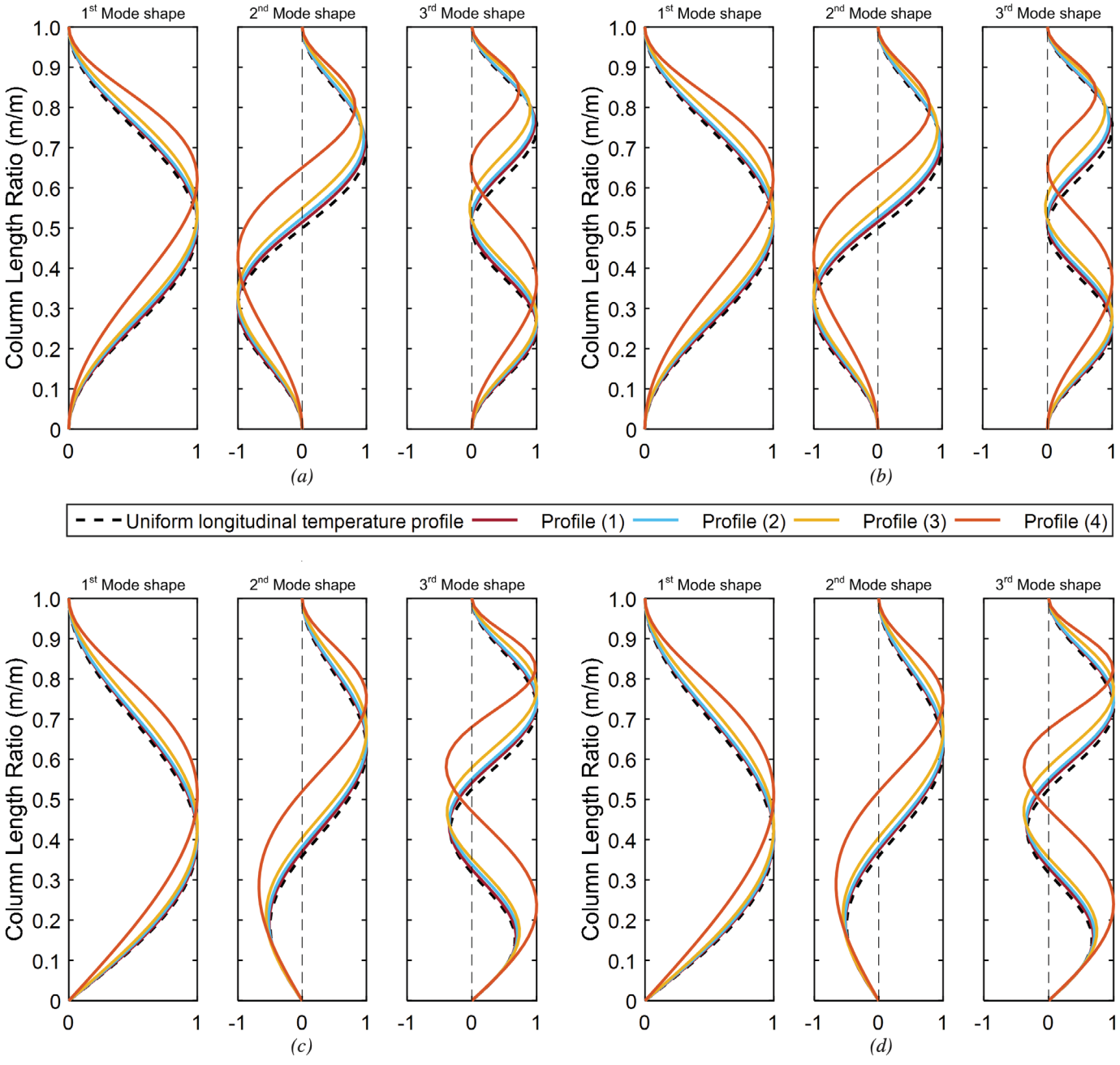


*Fig. 8. Comparison between (a) linear temperature distribution and fixed-fixed BC, (b) parabolic temperature distribution and fixed-fixed BC, (c) linear temperature distribution and pinned-fixed BC, and (d) parabolic temperature distribution and pinned-fixed BC.*

| Table 3. Effective Length Factors, *K*, for Parabolic and Linear Longitudinal Variation of Temperature | | | | | | | | |
|---|---|---|---|---|---|---|---|---|
| Profiles | Pinned-Pinned | | Fixed-Fixed | | Fixed-Pinned | | Pinned-Fixed | |
| | Parabolic | Linear | Parabolic | Linear | Parabolic | Linear | Parabolic | Linear |
| Uniform longitudinal | 1.00 | | 0.50 | | 0.70 | | 0.70 | |
| 1 | 1.00 | 1.00 | 0.52 | 0.52 | 0.70 | 0.68 | 0.70 | 0.70 |
| 2 | 1.00 | 1.00 | 0.50 | 0.50 | 0.68 | 0.68 | 0.72 | 0.72 |
| 3 | 1.00 | 1.00 | 0.54 | 0.52 | 0.68 | 0.68 | 0.74 | 0.74 |
| 4 | 1.00 | 1.00 | 0.48 | 0.46 | 0.56 | 0.56 | 0.80 | 0.80 |

the expected ratio of elastic buckling stress for fixed-fixed, fixed-pinned, and pinned-fixed to that of the pinned-pinned boundary condition with minimal difference.

The effects of various nonuniform longitudinal temperature profiles are also studied in order to determine an appropriate equation for the Euler elastic buckling stress. This analysis is performed using nonuniform longitudinal linear temperature profiles and a pinned-pinned boundary condition. The results shown in Figure 9 indicate that the Euler elastic buckling stress varies from one profile to another. The ratio of Euler elastic buckling stress to yield stress corresponding to maximum temperature increases from profile 1, with smaller high temperature, to profile 4, with larger high temperature at the boundaries.

In this section, an equation is proposed to predict Euler elastic buckling stress in a steel W-shape column subjected to nonuniform longitudinal temperature distribution. The format of the equation (Equation 18) is identical to that of the Euler elastic buckling equation (Equation 16); however, an equivalent modulus of elasticity (shown in Equation 19) is considered instead of a constant modulus of elasticity to account for nonuniform longitudinal temperature profiles as follows:

$$F_e(T) = \frac{\pi^2 E_{eq}}{\lambda^2} \tag{18}$$

$$E_{eq} = e^{\left[\xi_1 \ln(E_{cool-end}) + \xi_2 \ln(E_{hot-end})\right]} \tag{19}$$

where $E_{cool\text{-}end}$ and $E_{hot\text{-}end}$ are modulus of elasticity at the cool and hot ends of the column, respectively. In addition, $\xi_1$ and $\xi_2$ are two unknowns determined by using multilinear regression analysis based on both parabolic and linear longitudinal temperature distributions per Equation 20:

$$\xi_1 = 0.4815, \xi_2 = 0.5226 \tag{20}$$

Therefore, the Euler elastic buckling stress can be predicted according to Equation 21 for nonuniform longitudinal temperature profiles. It is noted that the effective length factor of uniform longitudinal temperature distribution was

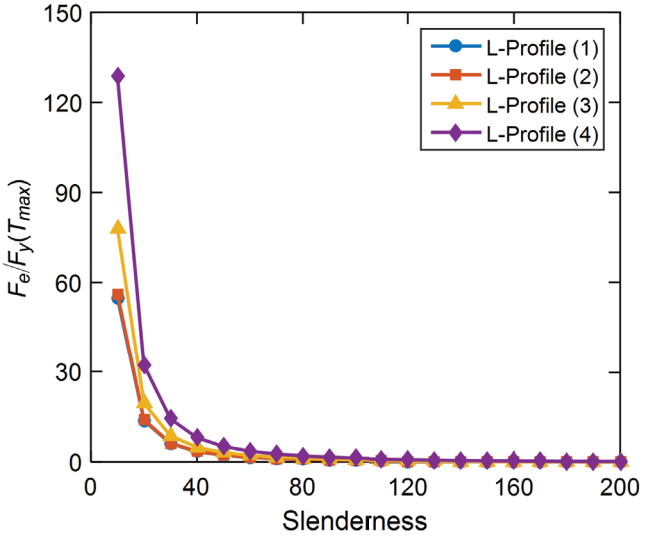


*Fig. 9. The effects of various longitudinal temperature profiles on Euler elastic buckling stress.*

inherently considered in the regression analysis; therefore, the $K$ factor for ambient temperature must be used in the proposed equation. Figure 10 shows the accuracy of Equation 21 in predicting the Euler elastic buckling stress for longitudinal temperature profiles 1 and 3 when considering pinned-pinned and fixed-pinned boundary conditions, respectively. It is observed that the error in the proposed equation for profile 1 with a pinned-pinned boundary condition is less than 4% in comparison with the results of finite element analysis. In addition, the proposed equation predicts the Euler elastic buckling stress for profile 3 with an error between 13 and 16% compared with the results of finite element analysis.

$$F_e(T) = \frac{\pi^2}{\lambda^2} e^{\left[0.4815\ln(E_{cool-end})+0.5226\ln(E_{hot-end})\right]} \qquad (21)$$

It should be emphasized that the proposed equation was extracted based on the analyses conducted on the nonuniform longitudinal temperature profiles considered in the current study. This equation can also provide a prediction of Euler elastic buckling stress in other cases of nonuniform longitudinal temperature profiles. This will be investigated later by conducting an analysis on a steel column subjected to two other nonuniform linear longitudinal temperature profiles, called profiles 5 and 6.

## NONLINEAR INELASTIC ANALYSIS

To determine the critical buckling stress causing column instability, the applied compressive force is increased incrementally until the onset of buckling in the column. A compact W14×90 section, fabricated from ASTM A572-Grade 50 steel, is selected for the nonlinear inelastic analysis. As indicated in the AISC *Specification* (AISC, 2016), columns with slenderness ratio $\lambda$ less than $4.71\sqrt{\frac{E}{F_y}}$ at ambient temperature are susceptible to inelastic buckling, while columns with slenderness greater than $4.71\sqrt{\frac{E}{F_y}}$ buckle elastically. Therefore, it is important that this distinction be captured in the finite element analysis of the column. This is realized by defining two independent limit states. For the inelastic buckling, the onset of compressive yielding at the cross-section of the steel column, based on the temperature-dependent yield stress at any section, is chosen as the limit state for the inelastic buckling. Furthermore, the calculated stress in the cross-section is influenced not only by the applied load, but also by any residual stresses that might be present, modeled by the residual stress field shown in Figure 11. It is assumed that the maximum thermally induced residual stresses are 10 ksi (~70 MPa) at ambient temperature (Takagi and Deierlein, 2007). The reduction factor for

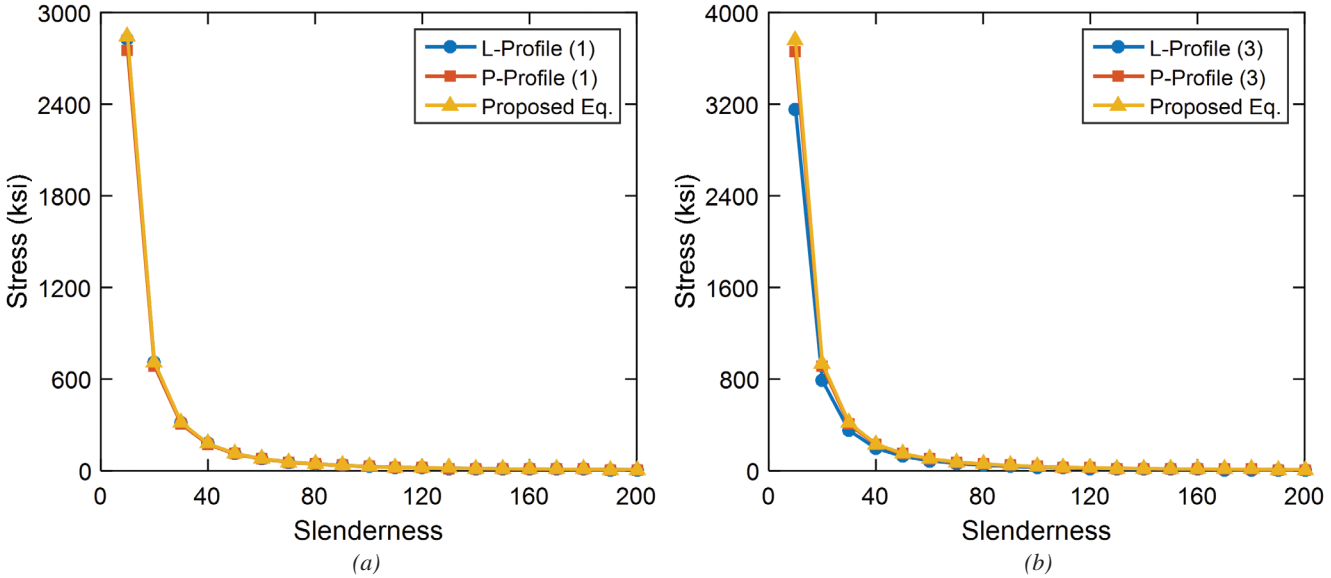


*Fig. 10. Euler elastic buckling stress computed by finite element analysis and proposed equation based on (a) pinned-pinned boundary condition in profile 1 and (b) fixed-pinned boundary condition in profile 3.*

yield stress at elevated temperatures is also used to reduce the intensity of the residual stresses in the cross section. This assumption was also made by Takagi and Deierlein.

To determine the elastic buckling, the lateral stiffness of the column at a given loading increment is computed; it is then compared to the initial lateral stiffness of the column, which is calculated based on first increment of loading. Initial assessment of the developed formulation indicates that the onset of elastic buckling is reached when the column loses 96% or more of its initial lateral stiffness. A set of analyses is conducted to verify the analysis approach in the current study. This includes examination of buckling of a pinned-pinned column at ambient and uniform longitudinal elevated temperatures using the W14×90 steel column considered previously. Details of the column evaluated are shown in Figure 12(a). The material model utilized is shown in Figure 3 for ambient and elevated temperatures. This matches the assumptions made in the AISC *Specification* (AISC, 2016) for column buckling stress in Section E and Appendix 4 for ambient and elevated temperatures, respectively. Furthermore, while column initial out-of-straightness is considered, the effect of out-of-plumbness is neglected in the verification analysis because it is not reflected in the AISC *Specification* for critical buckling stress of members under compressive forces.

At ambient temperature, the results of the finite element analysis are compared to the column buckling stress, $F_{cr}$, determined with AISC *Specification* Equations E3 and E4 (AISC, 2016). As shown in Figure 12(b), excellent agreement is observed between the critical buckling stresses computed using finite element analysis and that of the AISC *Specification* design equation. Verification of column stability at elevated temperatures is utilized by the column buckling equations at elevated temperature, proposed by Takagi and Deierlein (2007), available in AISC *Specification* Appendix 4. The comparison is conducted at two temperatures of 752°F (400°C) and 1472°F (800°C). Very good agreement is also observed between the results obtained by finite element formulation and the equation available in AISC *Specification* Appendix 4, as shown in Figures 12(c) and 12(d).

A parametric study is performed on a steel column with pinned-pinned boundary conditions, shown in Figure 13, using four nonuniform longitudinal temperature profiles, according to Figure 5. Figure 14 shows the critical buckling stress of a pinned-pinned steel column subjected to various nonuniform longitudinal temperature profiles. It is observed that there is an insignificant difference between the critical buckling stress of parabolic and linear nonuniform longitudinal temperature profiles. In addition, various nonuniform temperature profiles result in different buckling response with respect to the column slenderness. Figure 14 also shows that the ratio of critical buckling stress to yield

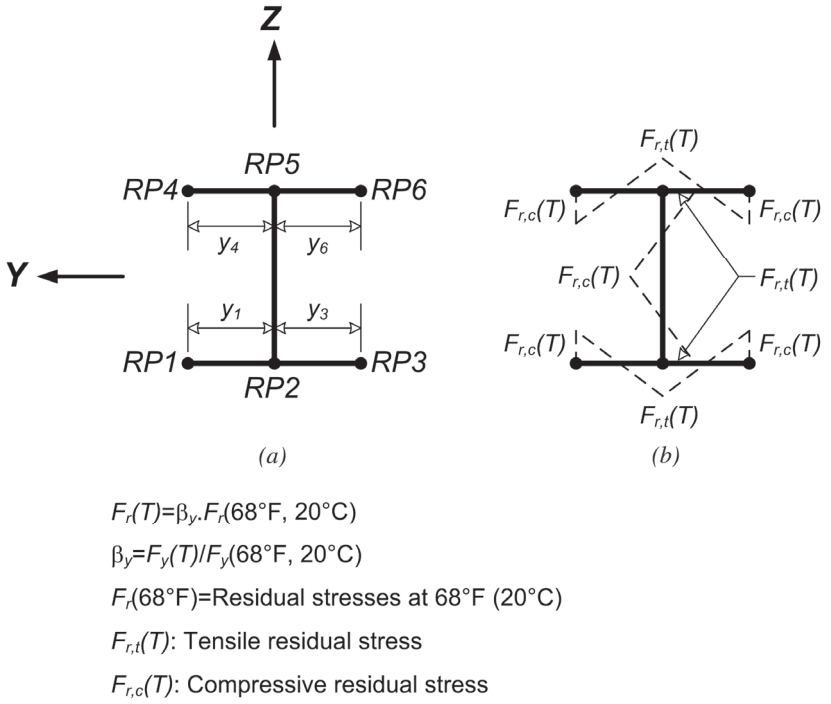


*Fig. 11. (a) Six reference points (RPs) and (b) distribution of residual stresses in a W-shape hot-rolled steel section.*

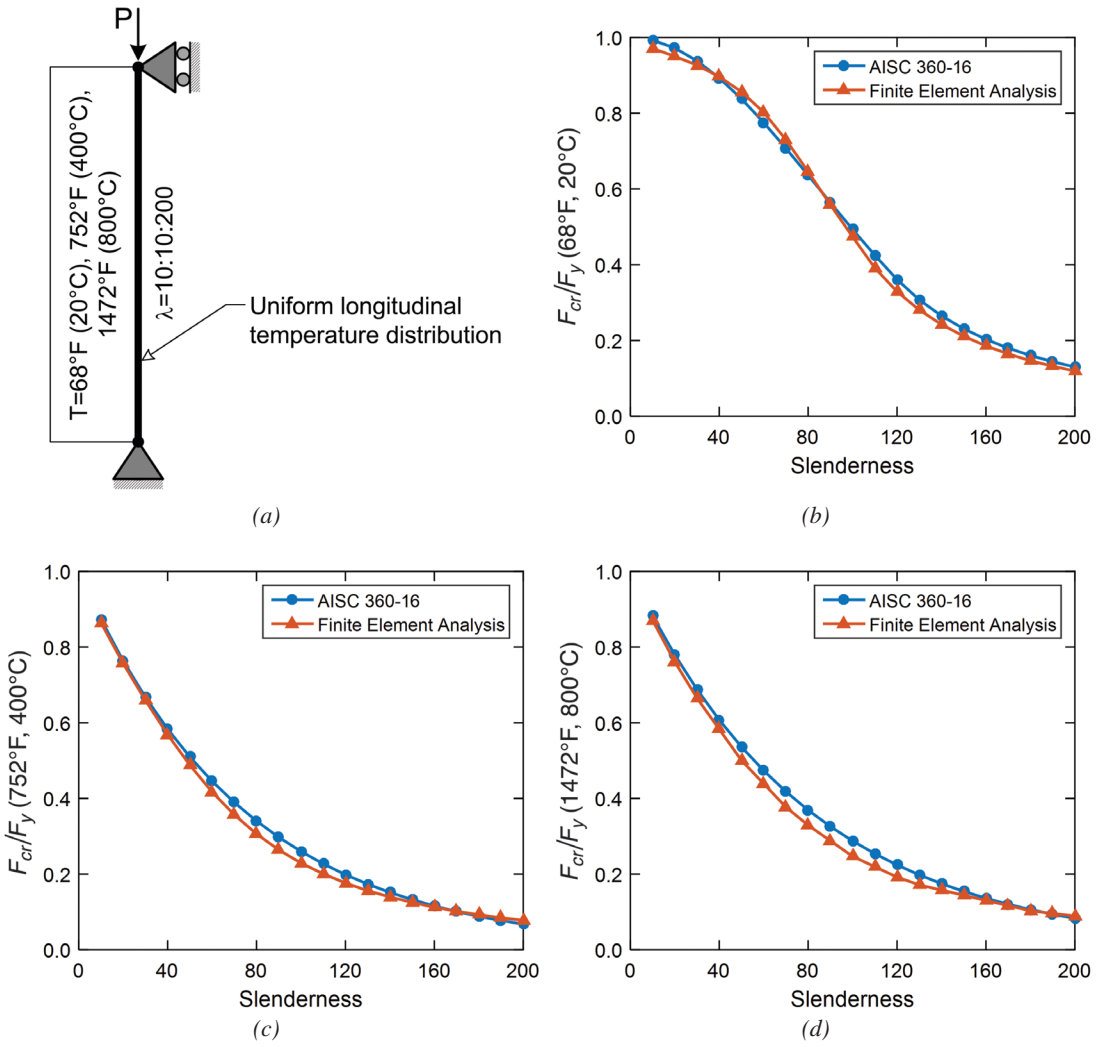


*Fig. 12. (a) Steel column subjected to a uniform longitudinal temperature and buckling stress computed using AISC* Specification *(AISC, 2016) and finite element analysis at (b) ambient temperature, (c) 752°F (400°C), and (d) 1472°F (800°C).*

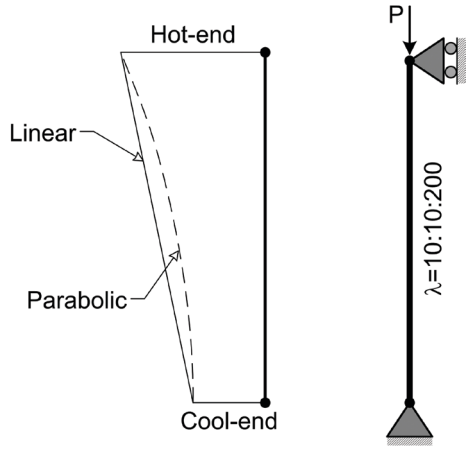


*Fig. 13. (a) Nonuniform parabolic and linear longitudinal temperature profiles; (b) pinned-pinned column with various slenderness ratios.*

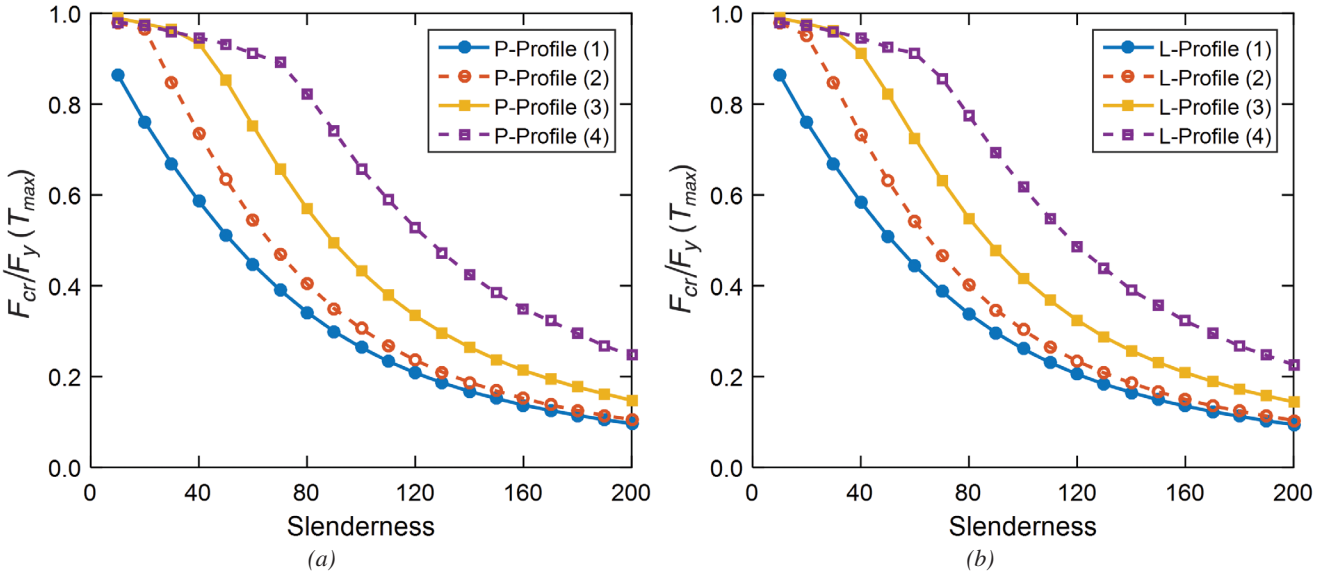


*Fig. 14. Critical buckling stress in the pinned-pinned steel column with (a) parabolic and (b) linear nonuniform longitudinal temperature profiles.*

stress corresponding to maximum temperature in the column increases with an increase in the maximum temperature of the column as this ratio decreases from profile 4 to profile 1.

## PROPOSED DESIGN EQUATION

This section discusses a proposal for an equation to predict the critical buckling stress of steel columns subjected to nonuniform longitudinal temperature profiles. The proposed equation allows structural engineers to estimate the nominal strength of steel columns subjected to fire loads. The proposed equation has a similar format to the current equation listed in AISC *Specification* Appendix 4 (AISC, 2016) proposed by Takagi and Deierlein (2007). Two coefficients, $p$ and $q$, are added to the current design equation in the AISC *Specification* to consider longitudinal variation of mechanical properties of structural steel shown in Equation 22:

$$F_{cr}(T) = \left[ (0.42p) \sqrt[q]{\left( F_y(T_{\max}) / F_e(T) \right)^q} \right] F_y(T_{\max}) \qquad (22)$$

where $F_e(T)$ is calculated according to Equation 21. Two coefficients, $p$ and $q$, depend on temperature profiles as listed in Tables 4 and 5. The term $F_y(T_{max})$ corresponds to the yield stress at the hot end of the column. In addition, coefficients $p$ and $q$ can be considered as unity for uniform longitudinal temperature profiles to convert Equation 22 to the current available design equation in AISC *Specification* Appendix 4.

As shown in Figure 15, the proposed equation is in

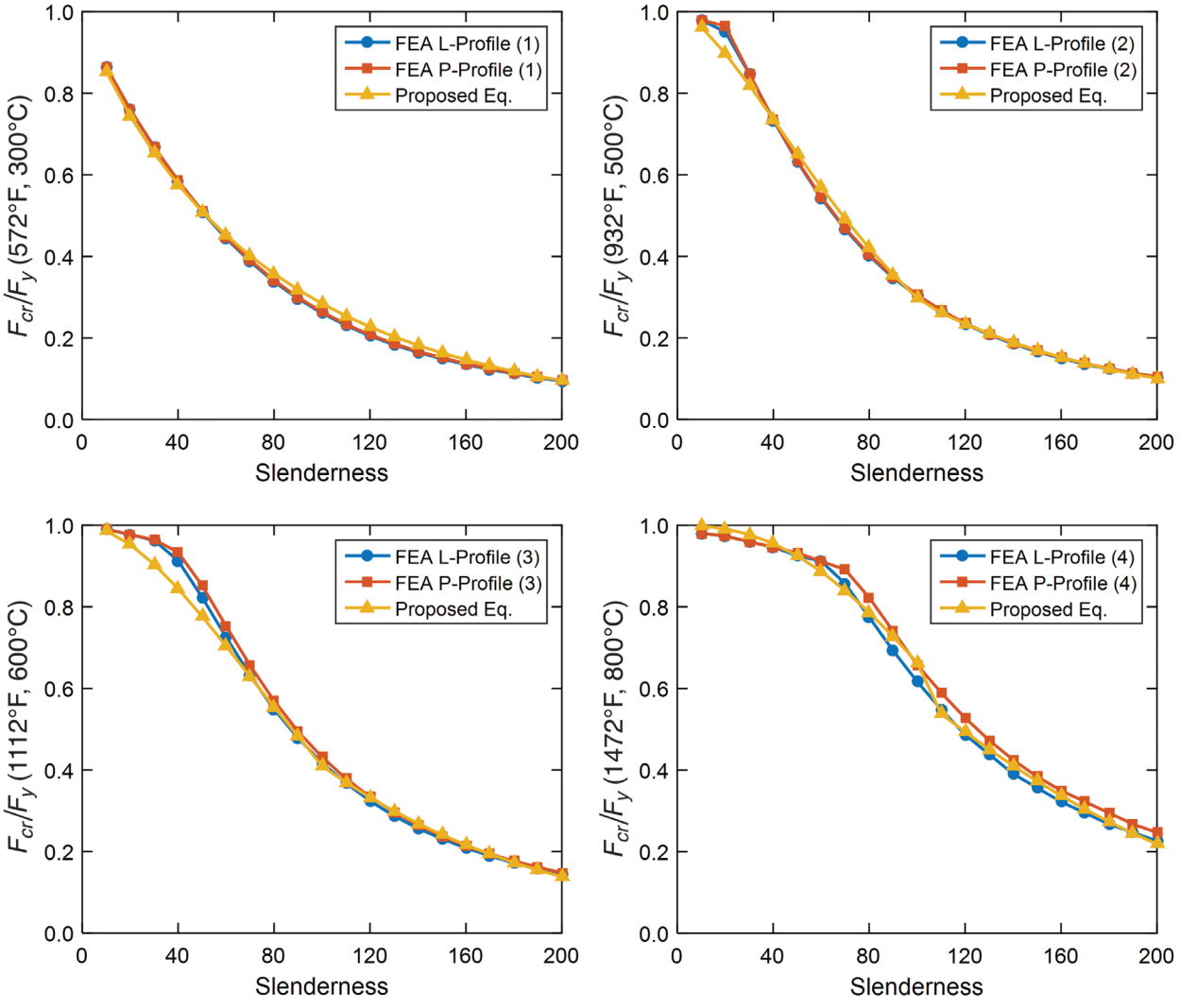


*Fig. 15. Critical buckling stress computed by FEA and the proposed equation.*

| Table 4. $p$ and $q$ Coefficients for $\lambda \le 4.71\sqrt{\frac{E(T_{max})}{F_y(T_{max})}}$ | | | |
|---|---|---|---|
| **Profile** | **Longitudinal Variation of Yield Stress (%)** | ***p*** | ***q*** |
| 1 | 0.0 | 0.90 | 0.90 |
| 2 | 22.0 | 1.05 | 1.50 |
| 3 | 53.0 | 1.30 | 1.80 |
| 4 | 89.0 | 1.30 | 2.40 |

| Table 5. $p$ and $q$ Coefficients for $\lambda > 4.71\sqrt{\frac{E(T_{max})}{F_y(T_{max})}}$ | | | |
|---|---|---|---|
| **Profile** | **Longitudinal Variation of Yield Stress (%)** | ***p*** | ***q*** |
| (1) | 0.0 | 0.90 | 0.90 |
| (2) | 22.0 | 0.90 | 0.90 |
| (3) | 53.0 | 1.18 | 1.15 |
| (4) | 89.0 | 1.20 | 1.50 |

| Table 6. Longitudinal Variation of Mechanical Properties of Structural Steel According to Two New Nonuniform Temperature Profiles | | | | | |
|---|---|---|---|---|---|
| | | | **Longitudinal Variation of Mechanical Properties between Cool and Hot Ends of Steel Column (%)** | | |
| **Profile** | **Temperature at Cool End, °F (°C)** | **Temperature at Hot End, °F (°C)** | **Modulus of Elasticity, ksi** | **Yield Stress, ksi** | **Proportional Limit** |
| 5 | 68 (20) | 1472 (800) | 91.0 | 89.0 | 95.0 |
| 6 | 932 (500) | 1272 (700) | 78.3 | 70.5 | 79.2 |

excellent agreement with the results of the finite element analysis (FEA). The comparison between the predicted critical buckling stresses calculated using the proposed equation and the results of the finite element analysis indicates a relative error of less than 10% in all cases. The accuracy of the proposed equation will be evaluated later using two other nonuniform longitudinal temperature profiles—profiles 5 and 6.

## ADEQUACY EVALUATION OF THE PROPOSED EQUATIONS

This final section investigates the adequacy of the proposed equations in the current study by considering two new nonuniform longitudinal temperature profiles as shown in Table 6. In profile 5, longitudinal temperature varies from ambient temperature 68°F (20°C) to 1472°F (800°C) in a linear fashion. However, boundaries of profile 6 have ambient temperatures of 932°F (500°C) and 1272°F (700°C), which varies with a linear pattern along the length of the column. These two longitudinal temperature profiles were selected such that profile 5 represents an extreme longitudinal variation of temperature, and profile 6 allows for interpolating all coefficients introduced in the proposed equations. The characteristics of each profile are shown in Table 6. It is noted that the pinned-pinned mechanical boundary condition is also considered in the current analysis according to Figure 13.

A linear elastic analysis is conducted to compute the Euler elastic buckling stress using finite element analysis. In addition, the Euler elastic buckling stress is calculated using Equation 21. As indicated previously, this equation only considers the modulus of elasticity as a function of temperature at both ends of the column. The results of the analysis are shown in Figure 16 for profiles 5 and 6. It is observed that the proposed equation for Euler elastic buckling stress underestimates the stress with an approximate 35% relative error in profile 5. However, the relative error is about

2% in profile 6 when predicting the Euler elastic buckling stress. Because the analysis is elastic, these two errors are constant for all ranges of slenderness for profiles 5 and 6. It is concluded that the proposed equation for the Euler elastic buckling analysis (Eq. 21) demonstrates a good adequacy for nonuniform longitudinal temperature profiles, which falls within the range of nonuniform profiles considered in the current study according to Table 1.

A set of nonlinear inelastic analysis is also conducted to assess the adequacy of the proposed equation for determining the critical buckling stress of steel columns subjected to nonuniform longitudinal temperature profiles. To do so, the critical buckling stress is computed using both the finite element analysis and the proposed Equation 22. It should be noted that coefficients $p$ and $q$ are determined for these two new profiles based on a variation of yield stress using linear interpolation as necessary. The results of analysis are shown in Figure 17 for profiles 5 and 6. It is seen that the proposed Equation 22 underestimates the critical buckling stress for slenderness greater than 100 on average with an

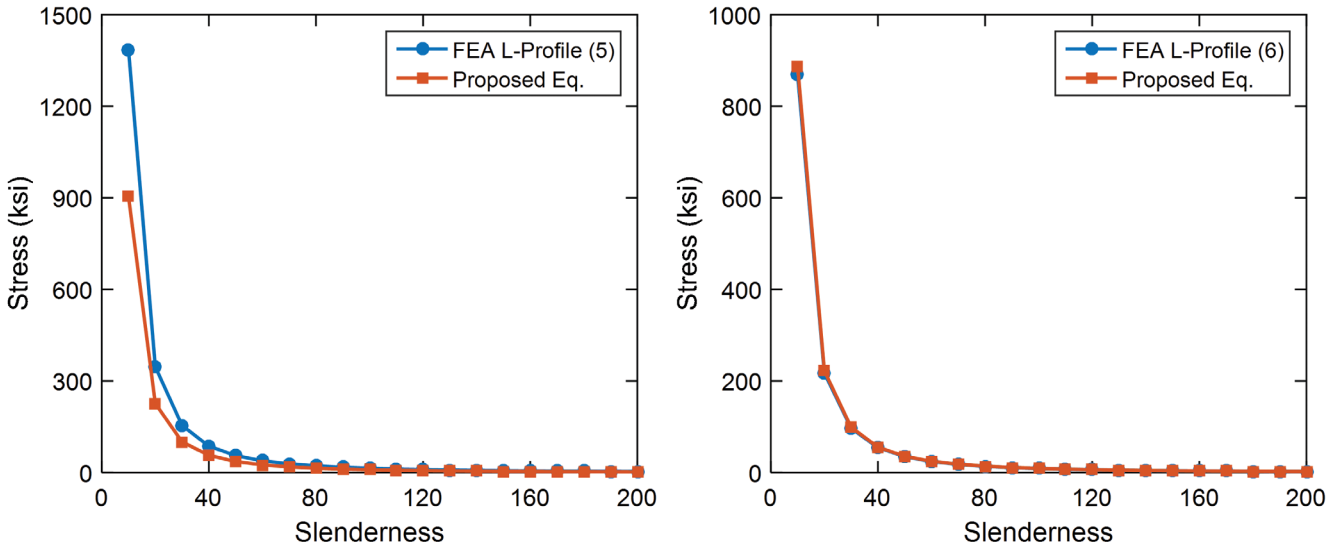


*Fig. 16. Adequacy of the proposed equation to predict Euler elastic buckling stress.*

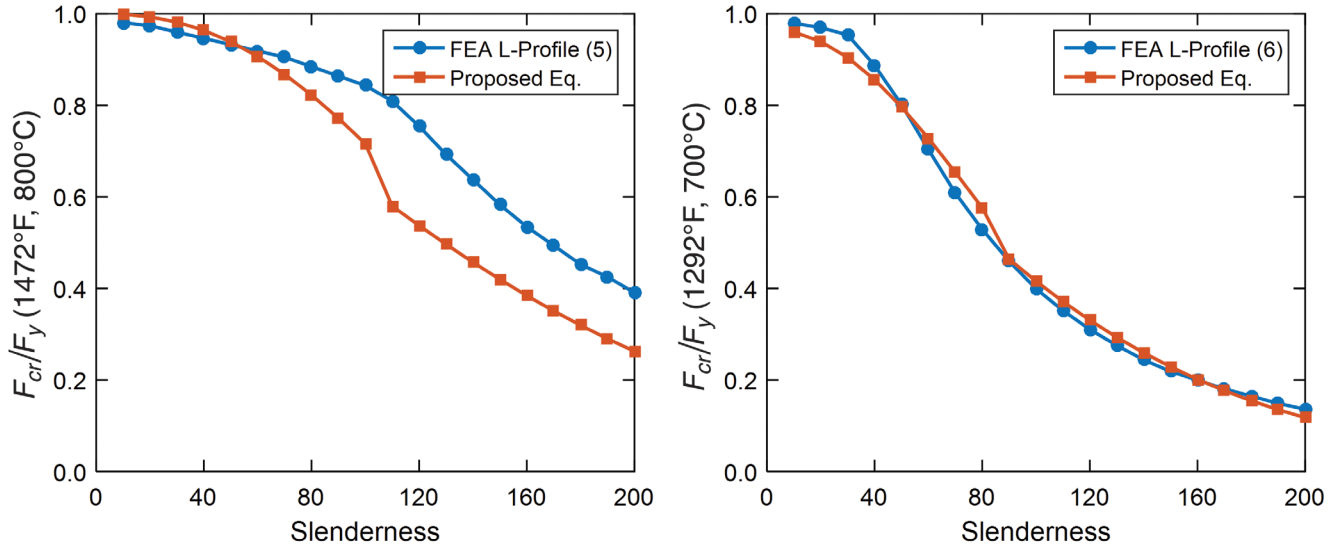


*Fig. 17. Adequacy of the proposed equation to predict the critical buckling stress in the steel columns subjected to nonuniform longitudinal temperature profiles.*

approximate 30% relative error for profile 5. However, the maximum relative error for predicting the critical buckling stress is about 13% for profile 6, while the average relative error for predicting the critical buckling stress is approximately 5% for all ranges of slenderness. It is concluded that the proposed equation for the critical buckling stress, Equation 22, provides good adequacy for nonuniform longitudinal temperature profiles for the range of nonuniform profiles considered in the current study in accordance with Table 1. Moreover, a comparison between the design equations available in AISC *Specification* Appendix 4 (AISC, 2016) and the one proposed in the current study reveals that the current equation in the AISC *Specification* cannot accurately predict the buckling stress for nonuniform longitudinal temperature profiles if either the average or maximum temperatures are used.

## SUMMARY AND CONCLUSION

In this article, a nonlinear finite element approach was introduced for assessing the response of steel columns under fire loads. This methodology included $P$-$\delta$ and $P$-$\Delta$ effects, residual stresses in W-shape hot-rolled steel sections, temperature-dependent mechanical properties of material, various boundary conditions, and nonuniform temperatures along the length of the column. Four various nonuniform longitudinal temperature profiles were considered to allow for evaluating the effects of various rates of change in temperature-dependent mechanical properties of structural steel, including modulus of elasticity, yield stress, and proportional limit.

The following preliminary conclusions can be drawn from the linear elastic analysis:

- The Euler elastic buckling stress of W-shape steel columns, computed by finite element analysis, is in excellent agreement with results of the classical Euler elastic buckling equation. This verified both first-order and geometric stiffness matrices generated based on the finite element method.
- It is observed that the mode shapes of instability change from uniform to nonuniform longitudinal temperature profiles. This change is relatively significant in nonuniform longitudinal profile 4. In addition, the mode shapes indicate that maximum deflection along column length is shifted toward higher temperature zones (i.e., softer material) while naturally accounting for the effect of boundary conditions.
- The effective length factors for nonuniform longitudinal temperature profiles show a small change in profiles 1, 2 and 3 versus uniform longitudinal temperature as expected because the change in mode shapes is minimal. The change in effective length factors is relatively significant in profile 4.
- Insignificant difference is observed between parabolic and linear temperature profiles in the elastic response with respect to Euler elastic buckling stress, mode shapes of instability, and effective length factor.
- An equation is proposed to predict Euler elastic buckling stress in W-shape steel columns subjected to nonuniform longitudinal temperature distribution. The results of proposed equation indicate good agreement with the solution of the eigenvalue problem.
- Adequacy of the proposed equation is assessed using two new nonuniform longitudinal temperature profiles. It is concluded that the proposed equation reveals a good adequacy for nonuniform longitudinal temperature profiles, which falls within the range of nonuniform profiles considered in the present study.

The following conclusions can be drawn from the nonlinear inelastic analysis:

- The initial imperfections, including out-of-straightness and out-of-plumbness, are independently considered in the geometry of the columns analyzed.
- Good agreement is observed between results of the finite element approach and available strength design equations for steel columns at ambient and uniform longitudinal elevated temperatures per the AISC *Specification* (AISC, 2016).
- A design equation is proposed to estimate the critical buckling stress of W-shape steel columns for the case of nonuniform longitudinal temperature profiles.
- The proposed equations show a good agreement with the results of nonlinear finite element analysis. The comparison between the predicted critical buckling stresses calculated using the proposed equation and the results of the FEA indicated a relative error of less than 10% in all cases.
- The adequacy of the proposed equation is assessed using two other nonuniform longitudinal temperature profiles—namely, profiles 5 and 6. It is observed that the proposed equation can have a good adequacy for nonuniform longitudinal temperature profiles, especially within the range of nonuniform profiles studied in the present article.

## REFERENCES

Agarwal, A., Choe, L. and Varma, A.H. (2014), "Fire Design of Steel Columns: Effects of Thermal Gradients," *Journal of Constructional Steel Research*, Vol. 93, pp. 107–118.

Agarwal, A. and Varma, A.H. (2011), "Design of Steel Columns at Elevated Temperatures Due to Fire: Effects of Rotational Restraints," *Engineering Journal*, Vol. 48, No. 4, pp. 297–314.

AISC (2005), *Specification for Structural Steel Buildings*, ANSI/AISC 360-05, American Institute of Steel Construction, Chicago, IL.

AISC (2010), *Specification for Structural Steel Buildings*, ANSI/AISC 360-10, American Institute of Steel Construction, Chicago, IL.

AISC (2016), *Specification for Structural Steel Buildings*, ANSI/AISC 360-16, American Institute of Steel Construction, Chicago, IL.

Ali, F. and O'Connor, D. (2001), "Structural Performance of Rotationally Restrained Steel Columns in Fire," *Fire Safety Journal*, Vol. 36, pp. 679–691.

Carol, I. and Murcia, J. (1989), "Nonlinear Time-Dependent Analysis of Planar Frames Using an Exact Formulation—I. Theory," *Computers and Structures*, Vol. 33, No. 1, pp. 79–87.

CEN (2005), *Eurocode 3: Design of Steel Structures—Part 1-2: General Rules—Structural Fire Design*, European Committee for Standardization.

Franssen, J.M., Talamona, D., Kruppa, J. and Cajot, L.G. (1998), "Stability of Steel Columns in Case of Fire: Experimental Evaluation," *Journal of Structural Engineering*, Vol. 124, No. 2, pp. 158–163.

Memari, M. (2016), "Performance of Steel Structures Subjected to Fire Following Earthquake," Ph.D. Dissertation, Colorado State University, Fort Collins, CO.

Memari, M. and Attarnejad, R. (2010), "An Innovative Timoshenko Beam Element," *Proceedings of the 10th International Conference on Computational Structures Technology*, Civil-Comp Press, Stirlingshire, U.K.

Memari, M. and Mahmoud, H. (2014), "Performance of Steel Moment Resisting Frames with RBS Connections under Fire Loading," *Engineering Structures*, Vol. 75, pp. 126–138.

Memari, M., Mahmoud, H. and Ellingwood, B. (2014), "Post-Earthquake Fire Performance of Moment Resisting Frames with Reduced Beam Section Connections," *Journal of Constructional Steel Research*, Vol. 103, pp. 215–229.

Memari, M., Mahmoud, H. and Ellingwood, B. (2017), "Stability of Steel Columns Subjected to Earthquake and Fire Loads," in press, *Journal of Structural Engineering.*

Moinuddin, K.A.M., Al-Menhali, J.S., Prasannan, K. and Thomas, I.R. (2011), "Rise in Structural Steel Temperatures during ISO 9705 Room Fires." *Fire Safety Journal*, Vol. 46, No. 8, pp. 480–496.

Morovat, M., Engelhardt, M., Helwig, T. and Taleff, E. (2014), "High-Temperature Creep Buckling Phenomenon of Steel Columns Subjected to Fire," *Journal of Structural Fire Engineering*, Vol. 5, No. 3, pp. 189–202.

Quiel, S.E. and Garlock, M.E. (2010), "Closed-Form Prediction of the Thermal and Structural Response of a Perimeter Column in a Fire," *The Open Construction and Building Technology Journa*l, Vol. 4, No. 1, pp. 64–78.

Stern-Gottfried, J., Rein, G., Bisby, L.A. and Torero, J.L. (2010), "Experimental Review of the Homogeneous Temperature Assumption in Post-Flashover Compartment Fires," *Fire Safety Journal*, Vol. 45, No. 4, pp. 249–261.

Takagi, J. and Deierlein, G.G. (2007), "Strength Design Criteria for Steel Members at Elevated Temperatures," *Journal of Constructional Steel Research*, Vol. 63, No. 8, pp. 1,036–1,050.

Tan, K.H. and Yuan, W.F. (2009), "Inelastic Buckling of Pin-Ended Steel Columns under Longitudinal Non-Uniform Temperature Distribution," *Journal of Constructional Steel Research*, Vol. 65, No. 1, pp. 132–141.

Vandamme, M. and Janss, J. (1981), "Buckling of Axially Loaded Steel Columns in Fire Conditions," *IABSE Proceedings*, P-43/81, IABSE Periodica 3/1981, pp. 81–95.

Wang, Y.C. (2002), *Steel and Composite Structures: Behaviour and Design for Fire Safety*, Taylor and Francis, Spon Press, New York, NY.

Witteveen, J. and Twilt L. (1981), "A Critical View on the Results of Standard Fire Resistance Tests on Steel Columns," *Fire Safety Journal*, Vol. 4, No. 4, pp. 259–270.

Zhang, C., Gross, J.L., McAllister, T.P. and Li, G.Q. (2014), "Behavior of Unrestrained and Restrained Bare Steel Columns Subjected to Localized Fire," *Journal of Structural Engineering*, Vol. 141, No. 10.